Magnetic MOF-808 as a novel adsorbent for toxic metal removal from aqueous solutions

Roxana Paz[a], Herlys Viltres[b*], Nishesh Kumar Gupta [c,d], Adolfo Romero-Galarza[e], Carolina

Leyva[a*]

[a]*Instituto Politécnico Nacional, Centro de Investigación en Ciencia Aplicada y Tecnología*

Avanzada, CDMX, México; [b]*School of Engineering Practice and Technology, McMaster*

University, Ontario, Canada; [c]*University of Science and Technology (UST), Daejeon, Republic*

of Korea; [d]*Department of Land, Water, and Environment Research, Korea Institute of Civil*

Engineering and Building Technology (KICT), Goyang, Republic of Korea; [e]*Department of*

Chemical Engineering, School of Chemistry, Universidad Autónoma de Coahuila, México

Section S1: Analytical instruments

For PXRD analysis, a PANalytical Empyream (United States) diffractometer was used. The

patterns were recorded with CuKα radiation (1.54183 Å) at 40 kV and 30 mA with a step size of

0.026 and a counting time of 0.4 s per point. FTIR spectra collection in a range of 400–4000 cm^{-1}

with 20 scans at a resolution of 4 cm^{-1} was carried out using a Perkin-Elmer (USA) instrument.

Raman spectra were collected by an XRD Thermo Fisher Scientific (United States) Raman

Microscope. A 780 nm excitation line in backscattering geometry through a 10× objective lens

was used to excite the samples with a power of ~6 mW (5 s of exposure time and 20 scans for each

recorded spectrum). The magnetization curves were recorded at 300 K using an MPMS-3

superconducting quantum interference device magnetometer. To evaluate the thermal stability of

the materials was used a T A Instruments, Q5000 IR model (United States), at a heating rate of 10

°C min^{-1} under N$_2$ flow. The evaluation of the superficial charge was measured by zeta potential

in a pH 2-6 range using NanoPlus HD sizer equipment (Micrometrics, United States) with a

minimum of 3 measurements per sample at room temperature. The X-ray photoelectron spectroscopy (XPS) analyses were carried out by a K-alpha Thermo Scientific spectrometer (United Kingdom). A spectrometer equipped with a hemispherical analyzer and a monochromatic AlKα X-ray source (1486.6 eV) in the Constant Analyzer Energy (CAE) was used for the study. Spectral backgrounds were subtracted using the Shirley method using CasaXPS software (version 2.3.14), and. The base pressure in the analyzer chamber was 1×10^{-9} mBar. Survey scans were recorded using 400 μm spot size and fixed pass energy of 200 eV, whereas high-resolution scans were collected at 20 eV of pass energy. Spectra have been charged corrected to the C 1s spectrum (adventitious carbon) set to 284.8 eV. The Hg(II) concentrations values were determined by triplicate of each sample using an Inductively Coupled Plasma Mass Spectrometer Optima 8000 (ICP-OES, Perkin Elmer, United States).

Section S2: Adsorption Experiments

Table S1. Summary of experimental conditions for Hg(II) adsorption experiments using the magnetic MOF (Zr-MOF@Fe$_3$O$_4$) as adsorbent.

[Dye]/mg·L^{-1}	**100**		
m(adsorbent)/mg	30	90	30
Volume/mL	30	90	30
	Sorbent dosage (mg)	**pH**	**Time**	**Adsorption Isotherm/mg·L^{-1}**
	10	2	30	30
	30	3	60	50

	50	4	90	100
	70	5	120	150
		6	180	250
			240	350
			720	
			1440	

Section S3: Materials characterization
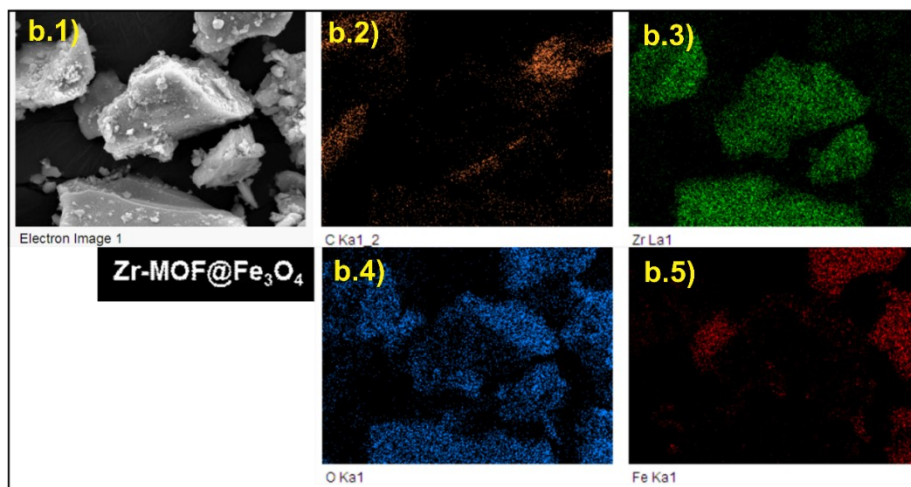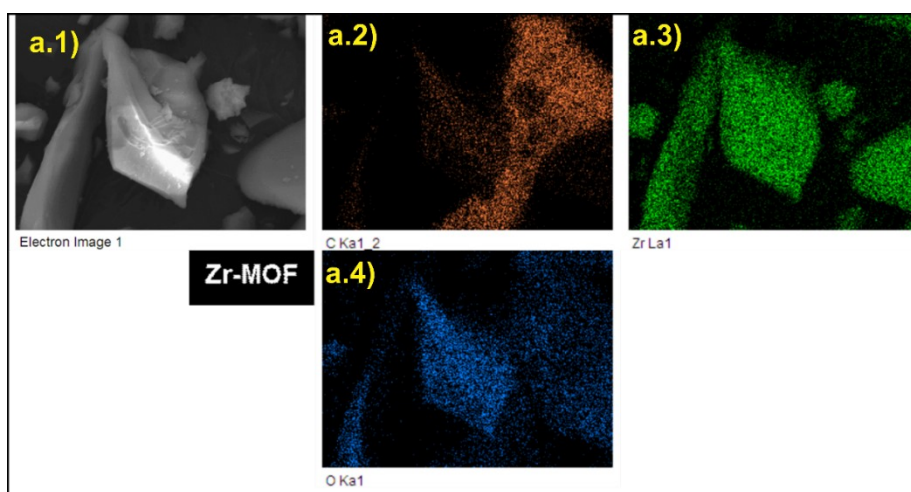
Figure S1. SEM micrographs and 2D elemental mapping of a) Zr-MOF and b) Zr-MOF@Fe$_3$O$_4$.
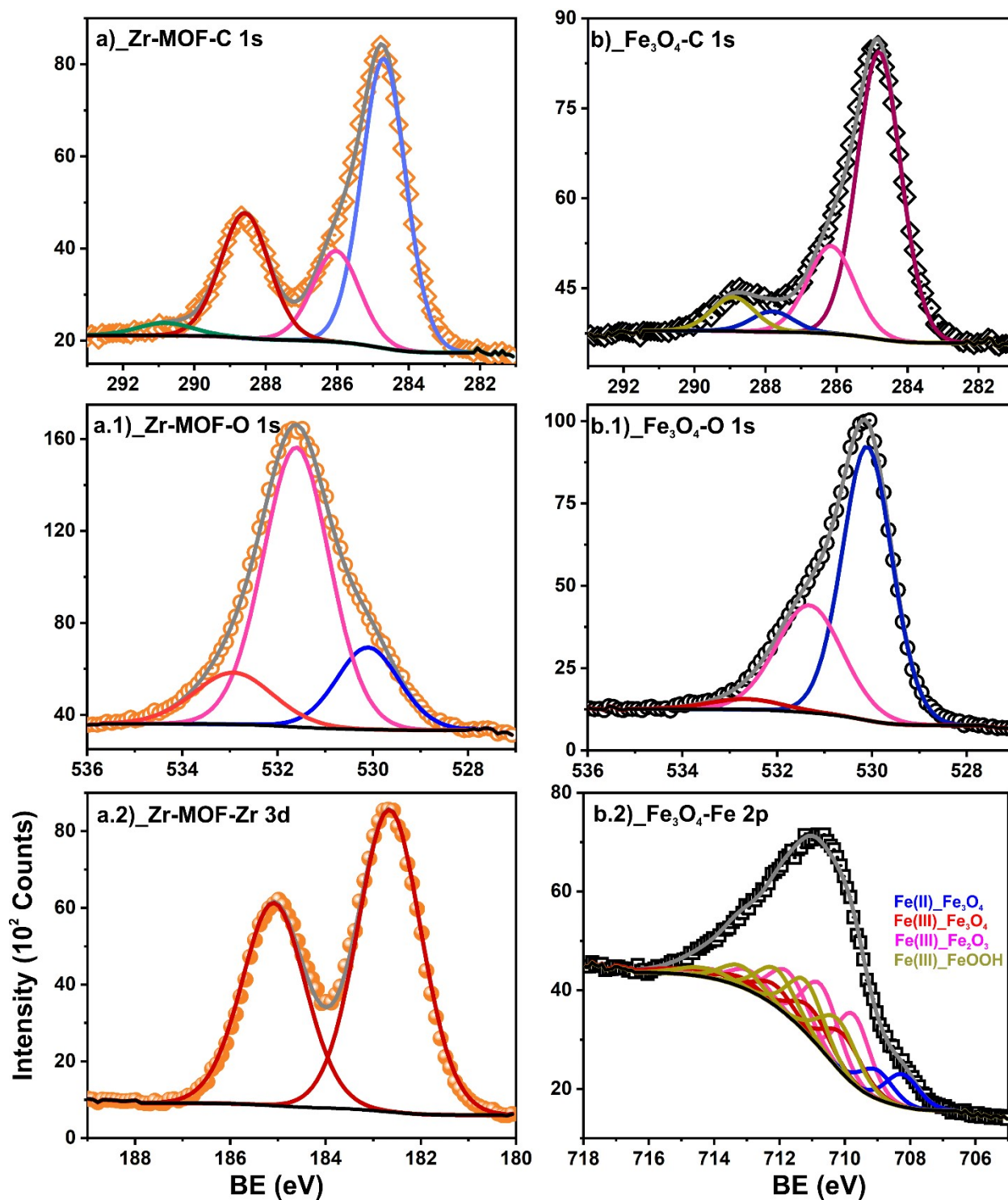
Figure S2. HRXPS (**a**) C 1s; (**a.1**) O 1s; (**a.2**) Zr 3d spectra of Zr-MOF; (**b**) C 1s; (**b.1**) O 1s; (**b.2**) Fe 2p spectra of Fe$_3$O$_4$.

Table S2. VSM analysis of Fe_3O_4 and Zr-MOF@Fe_3O_4 at T = 300 K.

Parameters	Fe_3O_4	Zr-MOF@Fe_3O_4
μ_s (emu g^{-1})	69.29	25.02
H_c (Oe)	8.70	5.18
μ_r (emu g^{-1})	0.74	0.15

Section S4: Hg(II) adsorption
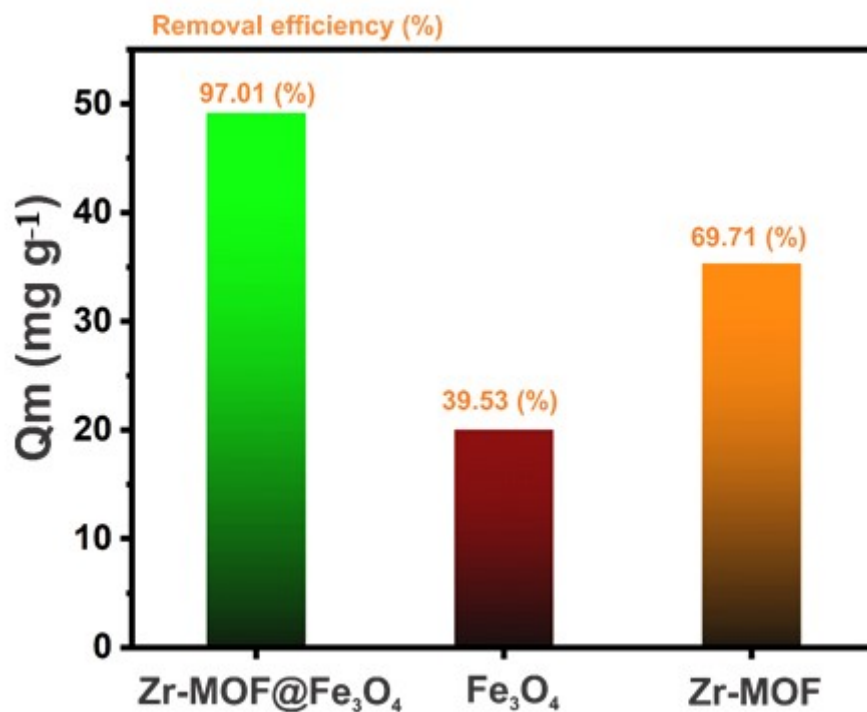
Figure S3. Control experiment of Hg(II) adsorption, Zr-MOF@Fe_3O_4, Fe_3O_4, and Zr-MOF.

Table S3. XPS survey data (atomic percentage) for the most concentrated elements for the materials.

Samples	Elements (At. %)		

	C 1s	O 1s	Zr 3d	Cl 2p	N 1s	S 2p	Fe 2p	Hg 4p
H$_3$BTC	67.8	32.2	-	-	-	-	-	-
Zr-Salt	36.7	30.6	13.3	19.5	-	-	-	-
Zr-MOF	56.8	34.7	7.3	1.2	-	-	-	-
Fe$_3$O$_4$	17.3	48.2	-	0.4	0.7	0.3	33.0	-
Zr-MOF@Fe$_3$O$_4$	34.0	41.7	4.6	-	-	-	19.8	-
Zr-MOF@Fe$_3$O$_4$ + Hg(II)	33.7	45.0	2.8	-	-	-	17.8	0.7

Table S4. The peak-fitting results of C 1s high-resolution signal of materials.

Samples	Assignment	E$_B$ (eV)	FWHM (eV)	At. %
Zr-MOF	C1s $_{C=C\ aromatic}$	284.7	1.4	53.5
	C1s $_{C-O}$	286.0	1.5	18.0
	C1s $_{O-C=O}$	288.6	1.6	25.5
	C1s $_{Satellite}$	290.8	1.8	3.0
Fe$_3$O$_4$	C1s $_{C-C}$	284.8	1.4	66.1
	C1s $_{C-O}$	286.1	1.5	21.6
	C1s $_{C??}$	287.8	1.4	4.6
	C1s $_{O-C=O}$	288.9	1.4	7.7
Zr-MOF@Fe$_3$O$_4$	C1s $_{C=C\ aromatic}$	284.7	1.4	55.8
	C1s $_{C-O}$	285.9	1.7	23.4

	C1s O-C=O	288.6	1.8	16.4
	C1s Satellite	290.7	1.9	4.4
Zr-MOF@Fe₃O₄ + Hg(II)	**C1s** C=C aromatic	284.7	1.5	47.3
	C1s C-O	285.9	1.7	30.0
	C1s O-C=O	288.4	1.8	12.9
	C1s Satellite	289.5	1.9	9.7

Table S5. The peak-fitting results of O 1s high-resolution signal of materials.

Samples	Assignment	E_B (eV)	FWHM (eV)	At. %
H₃BTC	**O1s** O-C=O	531.7	1.6	42.7
	O1s ₋C-OH	533.1	1.9	57.3
Zr-Salt	**O1s** O-Zr	530.6	1.5	22.0
	O1s Zr-OH	532.0	1.8	57.6
	O1s water	533.7	1.9	20.5
Zr-MOF	**O1s** O-Zr	530.1	1.5	18.3
	O1s O-C	531.6	1.6	63.5
	O1s Zr-OH	532.7	1.9	18.2
Fe₃O₄	**O1s** Fe-O	530.1	1.2	63.4
	O1s O-C	531.2	1.6	33.1
	O1s Fe-OH	532.7	1.8	3.5
Zr-MOF@Fe₃O₄	**O1s** O-Zr, O-Fe	530.2	1.5	50.4
	O1s O-C	531.7	1.6	37.7
	O1s Zr-OH	533.1	1.9	11.9

Zr-MOF@Fe$_3$O$_4$ + Hg(II)	**O1s** $_{\text{O-Zr, O-Fe}}$	530.3	1.5	36.8
	O1s $_{\text{O-C}}$	531.7	1.6	37.7
	O1s $_{\text{Zr-OH, Hg-OH}}$	533.1	1.9	25.5

Table S6. The peak-fitting results of Zr 3d$_{5/2}$ high-resolution signal of materials.

Samples	Assignment	E$_B$ (eV)	FWHM (eV)	At. %
Zr-Salt	**Zr3d** $_{\text{Zr-O}}$	183.2	1.7	100
Zr-MOF	**Zr3d** $_{\text{Zr-O}}$	182.7	1.6	100
Zr-MOF@Fe$_3$O$_4$	**Zr3d** $_{\text{Zr-O}}$	182.9	1.8	100
Zr-MOF@Fe$_3$O$_4$ + Hg(II)	**Zr3d** $_{\text{Zr-O}}$	183.2	1.9	100

Table S7. The peak-fitting results of Fe 2p$_{3/2}$ high-resolution signal of materials.

Samples	Assignment	E$_B$ (eV)	FWHM (eV)	At. %	Fe^{3+}/Fe^{2+} (Magnetite) (2:1)
Fe$_3$O$_4$	**Fe 2p$_{3/2}$** $_{\text{Fe(II)-Fe3O4}}$	708.2-709.1	1.2	10.0	2.1:1.0
	Fe 2p$_{3/2}$ $_{\text{Fe(III)-Fe3O4}}$	710-714.4	1.4-3.3	21.1	
	Fe 2p$_{3/2}$ $_{\text{Fe(III)-Fe2O3}}$	709.7-714.1	1.2-1.7	37.1	
	Fe 2p$_{3/2}$ $_{\text{Fe(III)-FeOOH}}$	710.1-714.3	1.4-1.8	31.8	
Zr-MOF@Fe$_3$O$_4$	**Fe 2p$_{3/2}$** $_{\text{Fe(II)-Fe3O4}}$	708.3-709.2	1.2	7.2	2.2:1.0
	Fe 2p$_{3/2}$ $_{\text{Fe(III)-Fe3O4}}$	710-713.4	1.4-3.3	15.7	
	Fe 2p$_{3/2}$ $_{\text{Fe(III)-Fe2O3}}$	709.6-714.1	1.2-1.7	11	
	Fe 2p$_{3/2}$ $_{\text{Fe(III)-FeOOH}}$	710.1-714.3	1.4-1.8	66.1	

Zr-MOF@Fe₃O₄ + Hg(II)	**Fe 2p₃/₂** Fe(II)-Fe3O4	708.2-709.2	1.2	4.3	2.2:1.0
	Fe 2p₃/₂ Fe(III)-Fe3O4	710-713.4	1.4-3.3	9.3	
	Fe 2p₃/₂ Fe(III)-Fe2O3	709.6-714.1	1.2-1.7	9.5	
	Fe 2p₃/₂ Fe(III)-FeOOH	710.1-714.3	1.4-1.8	76.9	

Table S8. The adsorption capacity of reported Zr-based MOFs for Hg(II) removal.

Adsorbent	Experimental conditions			q_e
	pH	Hg(II) (mg L⁻¹)	Time (h)	(mg g⁻¹)
PCN-221 [1]	7.1	50.00	0.5	233.60
UiO-66-NH₂ [2]	6.5	13.60	4.0	87.30
DUT-67 (Zr) [3]	6.0	0.02	2.0	0.04
Zr-MSA [4]	7.0	10.00	0.1	734.00
UiO-66-DMTD [5]	3.0	500.00	10.0	670.50
UiO-66-SH [6]	4.0	20.00	1.0	785.00
Thiol-modified Zr-DMBD [7]	6.0	500.00	6.0	171.50
Magnetic MOF-808 [This study]	6.0	350.00	24.0	302.95

Table S9. Kinetic model equations and parameters

Kinetic model	Linear equation	Parameter

PFO model	$$\log\left(q_e - q_t\right) = \log\left(q_e\right) - \left(\frac{k_{p1}}{2.303} * t\right)$$	qe: adsorption capacities at equilibrium (mg g^{-1}); qt: adsorption capacities at time t (mg g^{-1}); k_{p1}: pseudo-first-order rate constant for the kinetic model (mg g^{-1} min).
PSO model	$$\frac{t}{q_t} = \frac{1}{q_e^2 * k_2} + \frac{1}{q_e} * t$$ $$h = k_{p2} * q_e^2$$	qe: adsorption capacities at equilibrium (mg g^{-1}); qt: adsorption capacities at time t (mg g^{-1}); k_{p2}: pseudo-second-order rate constant of adsorption (mg g^{-1} min); h: initial adsorption rate (mg g^{-1} min^{-1}).
Elovich model	$$q_t = \frac{1}{\beta}\ln\left(\alpha * \beta\right) + \frac{1}{\beta}\ln(t)$$	qt: adsorption capacities at time t (mg g^{-1}); α: adsorption equilibrium constant (mg g^{-1} min^{-1}); β: equilibrium constant desorption (g mg^{-1}).
IPD model	$$q_t = k_{kip} * \sqrt{t} + C_i$$	qt: adsorption capacities at time t (mg g^{-1}); Kip: rate parameter of stage i (mg g^{-1} min$^{-1/2}$); Ci: intercept of stage i

		that gives an idea about of the thickness of boundary layer $(mg\ g^{-1})$.

Table S10. Kinetic parameters obtained for linear fitting of experimental adsorption data

Model	Parameter	Value
PFO model	$q_e\ (mg\ g^{-1})$	80.93
	$K_1\ (mg\ g^{-1}\ min)$	4.8×10^{-4}
	R^2	0.72
PSO model	$q_e\ (mg\ g^{-1})$	61.31
	$K_2\ (mg\ g^{-1}\ min^{-1})$	6.3×10^{-5}
	R^2	0.95
	h	0.24
Elovich model	$\beta\ (mg\ g^{-1})$	0.083
	$\alpha\ (mg\ g^{-1}\ min)$	0.75
	R^2	0.96
IPD model	$K_{ip1}\ (mg\ g^{-1}\ min)$	3.23
	$C_i\ (mg\ g^{-1})$	−11.66
	R^2	0.99
	$K_{ip2}\ (mg\ g^{-1}\ min)$	0.51
	$C_i\ (mg\ g^{-1})$	32.05
	R^2	0.81

Table S11. Adsorption isotherm equation and parameters

Isotherm	Non-linear equation	Parameter
Langmuir	$Q_e = \dfrac{Q_m K_L C_e}{1 + K_L C_e}$ $R_L = \dfrac{1}{1 + K_L C_o}$ $\Delta G(kJ/mol) = -RTlnKo$ $Ko = K_L * MM * 10^3$	Q_m is maximum adsorption capacity (mg g^{-1}); qe: amount of adsorbate in the adsorbent at equilibrium (mg g^{-1}); K_L is adsorption intensity or Langmuir coefficient (L mg^{-1}); R_L is separation factor; ΔG free Gibbs energy (kJ mol^{-1}). MM: Molar mass (g mol^{-1})
Freundlich	$Q_e = K_F C_e^{1/n}$	K_F is the constant indicative of the relative adsorption capacity (L g^{-1}) and n is indicative of the intensity
Dubinin-Radushkevich	$Q_e = q_s * e^{(-K_{ad} * \varepsilon^2)}$ $\varepsilon = RT * ln(1 + {}^1\!/C_e)$ $E = {}^1\!/\sqrt{2K_{ad}}$	K_{ad}: Dubinin–Radushkevich isotherm constant (mol^2 kJ^{-2}); q_e: amount of adsorbate in the adsorbent at equilibrium (mg g^{-1}); q_s: theoretical isotherm saturation capacity (mg g^{-1}); E is free energy per molecule of adsorbate (kJ mol^{-1})
Temkin	$Q_e = \dfrac{RT}{bt} * ln(At * Ce)$ $B = \dfrac{RT}{bt}$	At: Temkin isotherm equilibrium binding constant (L g^{-1}); bt: Temkin isotherm constant; R: universal gas constant (8.314J mol^{-1} K^{-1}); T: Temperature at 298 K; B:

		Constant related to heat of sorption (J mol^{-1})

Table S12. Adsorption isotherm parameters obtained for the non-linear fitting of experimental adsorption data.

Model	Parameter	Value
Langmuir	Q_m (mg g^{-1})	512.60
	K_L (L mg^{-1})	0.03
	R_L	0.09-0.64
	ΔG(kJ mol^{-1})	−21.33
	χ^2	109.92
	R^2	0.97
Freundlich	K_F (L g^{-1})	34.07
	n	1.79
	χ^2	31.49
	R^2	0.99
Dubinin-Radushkevich	K_{DR} (mol^2 kJ^{-2})	7.7×10^{-5}
	q_s (mg g^{-1})	45.58
	χ^2	3.56
	R^2	0.95
	E (kJ mol^{-1})	9.18
Temkin	A_t (L g^{-1})	3.29
	b_t	51.13

	B	48.43
	χ^2	419.19
	R^2	0.88

References

1   Z. Seyfi Hasankola, R. Rahimi, H. Shayegan, E. Moradi and V. Safarifard, Removal of Hg^{2+} heavy metal ion using a highly stable mesoporous porphyrinic zirconium metal-organic framework, *Inorganica Chim. Acta*, 2020, **501**, 119264.

2   Y. Zhao, D. Wang, W. Wei, L. Cui, C.-W. Cho and G. Wu, Effective adsorption of mercury by Zr(IV)-based metal-organic frameworks of UiO-66-NH_2 from aqueous solution, *Environ. Sci. Pollut. Res.*, 2021, **28**, 7068–7075.

3   S. Chen, F. Feng, S. Li, X.-X. Li and L. Shu, Metal-organic framework DUT-67 (Zr) for adsorptive removal of trace Hg^{2+} and CH_3Hg^+ in water, *Chem. Speciation Bioavailability*, 2018, **30**, 99–106.

4   P. Yang, Y. Shu, Q. Zhuang, Y. Li and J. Gu, A robust MOF-based trap with high-density active alkyl thiol for the super-efficient capture of mercury, *Chem. Commun.*, 2019, **55**, 12972–12975.

5   L. Fu, S. Wang, G. Lin, L. Zhang, Q. Liu, J. Fang, C. Wei and G. Liu, Post-functionalization of UiO-66-NH_2 by 2,5-Dimercapto-1,3,4-thiadiazole for the high efficient removal of Hg(II) in water, *J. Hazard. Mater.*, 2019, **368**, 42–51.

6   J. Li, Y. Liu, Y. Ai, A. Alsaedi, T. Hayat and X. Wang, Combined experimental and theoretical investigation on selective removal of mercury ions by metal organic frameworks modified with thiol groups, *Chem. Eng. J.*, 2018, **354**, 790–801.

7   L. Ding, X. Luo, P. Shao, J. Yang and D. Sun, Thiol-functionalized Zr-based metal–organic framework for capture of Hg(II) through a proton exchange reaction, *ACS Sustain. Chem. Eng.*, 2018, **6**, 8494–8502.